Letter

Crossed nonlinear dynamical Hall effect in twisted bilayers

Cong Chen [1,2,*] Dawei Zhai [1,2,*] Cong Xiao [2,3,†] and Wang Yao [1,2,‡]

[1]*New Cornerstone Science Laboratory, Department of Physics, University of Hong Kong, Hong Kong, China*
[2]*HKU-UCAS Joint Institute of Theoretical and Computational Physics at Hong Kong, Hong Kong, China*
[3]*Institute of Applied Physics and Materials Engineering, University of Macau, Taipa, Macau, China*

(Received 24 March 2023; accepted 23 January 2024; published 13 March 2024)

We propose a nonlinear dynamical Hall effect characteristic of layered materials with chiral symmetry, which is driven by the joint action of in-plane and time variation of out-of-plane ac fields $\boldsymbol{j}_{\mathrm{H}} \sim \dot{\boldsymbol{E}}_{\perp} \times \boldsymbol{E}_{\parallel}$. A different band geometric quantity—interlayer Berry connection polarizability, which probes a mixed quantum metric characteristic of layer hybridized electrons by twisted interlayer coupling—underlies this effect. When the two orthogonal fields have a common frequency, their phase difference controls the on/off, direction, and magnitude of the rectified Hall current. We show sizable effects in twisted homobilayer transition metal dichalcogenides and twisted bilayer graphene over a broad range of twist angles. Our work opens the door to discovering mixed quantum metric responses unique to van der Waals stacking and concomitant applications under the nonlinear spotlight.

DOI: 10.1103/PhysRevResearch.6.L012059

Introduction. Nonlinear Hall-type response to an in-plane electric field in a two-dimensional (2D) system with time-reversal symmetry has attracted marked interests [1–4]. Intensive studies have been devoted to uncovering new types of nonlinear Hall transport induced by quantum geometry [4–6] and their applications such as terahertz rectification [7] and magnetic information readout [8]. Restricted by symmetry [1], the known mechanisms of the nonlinear Hall response in quasi-2D nonmagnetic materials [2,3,9,10] are all of an extrinsic nature, sensitive to fine details of the disorders [11,12], which have limited their utilization for practical applications.

The intrinsic nonlinear Hall effect independent of scattering, on the other hand, has been attracting increasing interest [13–18], and the very recent observations of it in antiferromagnets spotlight the importance of exploring Hall transport induced by a quantum metric [19,20]. However, the intrinsic nonlinear Hall effect in its conventional paradigm [13] can only appear in magnetic materials.

Moreover, having a single driving field only, the conventional nonlinear Hall effect has not unleashed the full potential of nonlinearity for enabling a controlled gate in logic operation, where separable inputs (i.e., in orthogonal directions) are desirable. The latter, in the context of the Hall effect, calls for the control by both out-of-plane and in-plane electric fields. A strategy to introduce a quantum geometric response to an out-of-plane field in quasi-2D geometry is made possible in van der Waals (vdW) layered structures with twisted stacking [21–27] . Taking a homobilayer as an example, electrons have an active layer degree of freedom that is associated with an out-of-plane electric dipole [28–30], whereas interlayer quantum tunneling rotates this pseudospin about the in-plane axes that are of topologically nontrivial textures in the twisted landscapes [31–33]. Such layer pseudospin structures can underlie novel quantum geometric properties when coupled with an out-of-plane field.

In this Letter we unveil a different type of nonlinear Hall effect in time-reversal symmetric twisted bilayers, where an intrinsic Hall current emerges under the combined action of an in-plane electric field $\boldsymbol{E}_{\parallel}$ and an out-of-plane ac field $\boldsymbol{E}_{\perp}(t)$: $\boldsymbol{j} \sim \dot{\boldsymbol{E}}_{\perp} \times \boldsymbol{E}_{\parallel}$ [see Fig. 1(a)]. Having the two driving fields (inputs) and the current response (output) all orthogonal to each other, the effect is dubbed as the *crossed nonlinear dynamical Hall effect*. This is also a nonlinear Hall contribution of an intrinsic nature in nonmagnetic materials without an external magnetic field, determined solely by the band structures, not relying on extrinsic factors such as disorders and relaxation times. Having two driving fields of the same frequency, a dc Hall current develops, whose on/off, direction, and magnitude can all be controlled by the phase difference of the two fields. The effect has a band geometric origin in the momentum space curl of interlayer Berry connection polarizability (BCP), probes a mixed quantum metric arising from the interlayer hybridization of electronic states under the chiral crystal symmetry, and enables a unique phase tunable rectification in chiral vdW layered materials and a transport probe of them. As examples, we show sizable effects in small angle twisted transition metal dichalcogenides (tTMDs) and twisted bilayer graphene (tBG), as well as tBG of large angles where umklapp interlayer tunneling dominates.

Geometric origin of the effect. A bilayer system couples to in-plane and out-of-plane driving electric fields in completely different ways. The in-plane field couples to the 2D crystal

*These authors contributed equally to this work.
†congxiao@um.edu.mo
‡wangyao@hku.hk

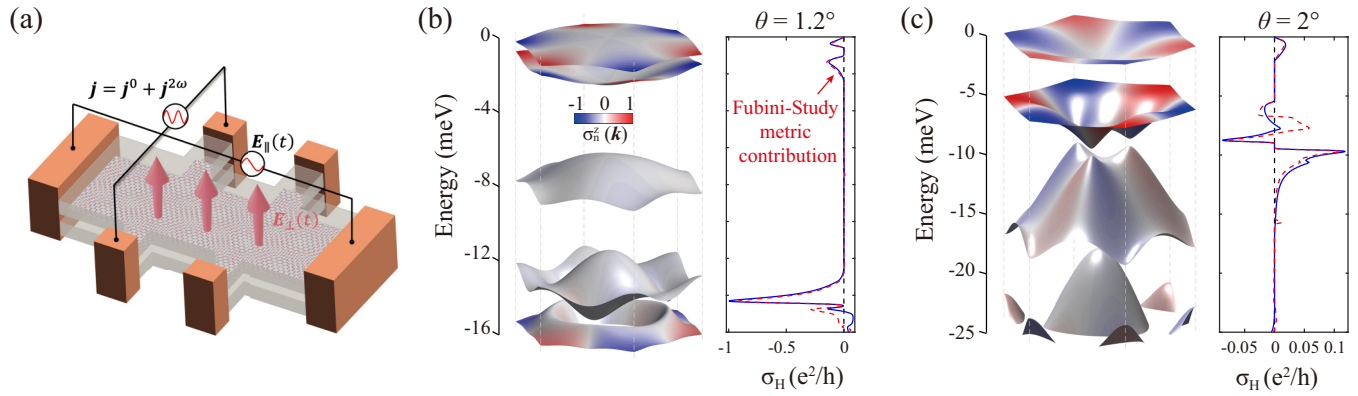

FIG. 1. (a) Schematics of the experimental setup. (b), (c) Valence-band structure and intrinsic Hall conductivity with respect to in-plane input for $tMoTe_2$ at twist angles (b) $\theta = 1.2°$ and (c) $\theta = 2°$ in the $+K$ valley. In (b) and (c) the color coding denotes the layer composition $\sigma_n^z(\boldsymbol{k})$, and the red dashed curve denotes the contribution of the Fubini-Study metric term.

momentum, leading to Berry-phase effects in 2D momentum space [34]. In comparison, the out-of-plane field is coupled to the interlayer dipole moment $\hat{p}$ in the form of $-E_\perp \hat{p}$, where $\hat{p} = ed_0\hat{\sigma}_z$ with $\hat{\sigma}_z$ as the Pauli matrix in the layer index subspace and d_0 the interlayer distance. When the system has a more than twofold rotational axis in the z direction, as in tBG and tTMDs, any in-plane current driven by the out-of-plane field alone is forbidden. It also prohibits the off-diagonal components of the symmetric part of the conductivity tensor $\sigma_{ab} = \partial j_a/\partial E_{\|,b}$ with respect to the in-plane input and output. Since the antisymmetric part of σ_{ab} is not allowed by the Onsager reciprocity in nonmagnetic systems, all the off-diagonal components of σ_{ab} are forbidden, irrespective of the order of the out-of-plane field. On the other hand, as we will show, an in-plane Hall conductivity $\sigma_{xy} = -\sigma_{yx}$ can still be driven by the product of an in-plane field and the time variation rate of an out-of-plane ac field.

To account for the effect, we make use of the semiclassical theory [13,34–36]. The velocity of an electron is given by

$$\dot{\boldsymbol{r}} = \frac{1}{\hbar}\partial_{\boldsymbol{k}}\tilde{\varepsilon} - \frac{e}{\hbar}\boldsymbol{E}_\parallel \times \boldsymbol{\Omega}_{\boldsymbol{k}} - \boldsymbol{\Omega}_{\boldsymbol{k}E_\perp}\dot{E}_\perp, \tag{1}$$

with $\hbar\boldsymbol{k}$ as the 2D crystal momentum. Here and hereafter we suppress the band index for simplicity, unless otherwise noted. For the velocity at the order of interest, the k-space Berry curvature $\boldsymbol{\Omega}_{\boldsymbol{k}}$ is corrected to the first order of the variation rate of out-of-plane field $\dot{E}_\perp$:

$$\boldsymbol{\Omega}_{\boldsymbol{k}} = \partial_{\boldsymbol{k}} \times (\boldsymbol{\mathcal{A}} + \boldsymbol{\mathcal{A}}^{\dot{E}_\perp}). \tag{2}$$

Here, $\boldsymbol{\mathcal{A}} = \langle u_{\boldsymbol{k}}|i\partial_{\boldsymbol{k}}|u_{\boldsymbol{k}}\rangle$ is the unperturbed k-space Berry connection, with $|u_{\boldsymbol{k}}\rangle$ being the cell-periodic part of the Bloch wave, whereas

$$\boldsymbol{\mathcal{A}}^{\dot{E}_\perp}(\boldsymbol{k}) = \boldsymbol{\mathcal{G}}(\boldsymbol{k})\dot{E}_\perp \tag{3}$$

is its gauge invariant correction [34,37,38], which can be identified physically as an in-plane positional shift of an electron [13] induced by the time evolution of the out-of-plane field. For a band with index n, we have (see details in the Supplemental Material [39])

$$\boldsymbol{\mathcal{G}}^n(\boldsymbol{k}) = 2\hbar^2\,\mathrm{Re}\sum_{m\neq n}\frac{p^{nm}(\boldsymbol{k})\boldsymbol{v}^{mn}(\boldsymbol{k})}{[\varepsilon_n(\boldsymbol{k}) - \varepsilon_m(\boldsymbol{k})]^3}, \tag{4}$$

whose numerator involves the interband matrix elements of the interlayer dipole and velocity operators, and ε_n is the unperturbed band energy.

Meanwhile, up to the first order of the in-plane field, the hybrid Berry curvature in $(\boldsymbol{k}, E_\perp)$ space reads $\boldsymbol{\Omega}_{\boldsymbol{k}E_\perp} = \partial_{\boldsymbol{k}}(\mathfrak{A} + \mathfrak{A}^{E_\parallel}) - \partial_{E_\perp}(\boldsymbol{\mathcal{A}} + \boldsymbol{\mathcal{A}}^{E_\parallel})$. Here, $\boldsymbol{\mathcal{A}}^{E_\parallel}$ is the k-space Berry connection induced by the $E_\parallel$ field [13,36], which represents an intralayer positional shift and whose detailed expression is not needed for our purpose. $\mathfrak{A} = \langle u_{\boldsymbol{k}}|i\partial_{E_\perp}|u_{\boldsymbol{k}}\rangle$ is the $E_\perp$-space Berry connection [42], and

$$\mathfrak{A}^{E_\parallel}(\boldsymbol{k}) = \frac{e}{\hbar}\boldsymbol{\mathcal{G}}(\boldsymbol{k}) \cdot \boldsymbol{E}_\parallel \tag{5}$$

is its first-order correction induced by the in-plane field. In addition, $\tilde{\varepsilon} = \varepsilon + \delta\varepsilon$, where $\delta\varepsilon = e\boldsymbol{E}_\parallel \cdot \boldsymbol{\mathcal{G}}\dot{E}_\perp$ is the field-induced electron energy [35].

Given that $\mathfrak{A}^{E_\parallel}$ is the $E_\perp$-space counterpart of intralayer shift $\boldsymbol{\mathcal{A}}^{E_\parallel}$, and that $E_\perp$ is conjugate to the interlayer dipole moment, we can pictorially interpret $\mathfrak{A}^{E_\parallel}$ as the interlayer shift induced by the in-plane field. It indeed has the desired property of flipping sign under the horizontal mirror-plane reflection, hence it is analogous to the so-called interlayer coordinate shift introduced in the study of the layer circular photogalvanic effect [42], which is merely the $E_\perp$-space counterpart of the shift vector well known in the nonlinear optical phenomenon of the shift current. Therefore, the $E_\perp$-space BCP $e\boldsymbol{\mathcal{G}}/\hbar$ can be understood as the interlayer BCP. This picture is further augmented by the connotation that the interlayer BCP is featured exclusively by interlayer-hybridized electronic states: According to Eq. (4), if the state $|u_n\rangle$ is fully polarized in a specific layer around some momentum $\boldsymbol{k}$, then $\boldsymbol{\mathcal{G}}(\boldsymbol{k})$ is suppressed.

With the velocity of individual electrons, the charge current density contributed by the electron system can be obtained from $\boldsymbol{j} = e\int[d\boldsymbol{k}]f_0\dot{\boldsymbol{r}}$, where $[d\boldsymbol{k}]$ is shorthand for $\sum_n d^2\boldsymbol{k}/(2\pi)^2$, and the distribution function is taken to be the Fermi function f_0 as we focus on the intrinsic response. The band geometric contributions to $\dot{\boldsymbol{r}}$ lead to a Hall current

$$\boldsymbol{j} = \chi^{\mathrm{int}}\dot{\boldsymbol{E}}_\perp \times \boldsymbol{E}_\parallel, \tag{6}$$

where

$$\chi^{\rm int} = \frac{e^2}{\hbar}\int [d\boldsymbol{k}] f_0 [\partial_{\boldsymbol{k}} \times \boldsymbol{\mathcal{G}}(\boldsymbol{k})]_z \tag{7}$$

is intrinsic to the band structure. This band geometric quantity measures the k-space curl of the interlayer BCP over the occupied states, and hence is also a characteristic of layer-hybridized electronic states. Via an integration by parts, it becomes clear that $\chi^{\rm int}$ is a Fermi-surface property. Since $\chi^{\rm int}$ is a time-reversal even pseudoscalar, it is invariant under rotation, but flips sign under space inversion, mirror reflection, and rotoreflection symmetries. As such, $\chi^{\rm int}$ is allowed if and only if the system possesses a chiral crystal structure, which is the very case of twisted bilayers [42,43]. Moreover, since twisted structures with opposite twist angles are mirror images of each other, whereas the mirror reflection flips the sign of $\chi^{\rm int}$, the direction of Hall current can be reversed by reversing the twist direction.

Quantum metric nature of the effect. Given the recent intensive studies on nonlinear Hall transport induced by the k-space quantum metric [19,20,44], it is interesting to point out that our proposed effect is ultimately related to the mixed quantum metric in $(\boldsymbol{k}, E_\perp)$ space, which is unique to 2D layered materials. The interlayer BCP can be cast into $\boldsymbol{\mathcal{G}}^n = -2\hbar\sum_{m\neq n}\boldsymbol{g}^{nm}/(\varepsilon_n - \varepsilon_m)$, where $\boldsymbol{g}^{nm} = {\rm Re}[\langle\partial_{E_\perp} u_n|u_m\rangle\langle u_m|\partial_{\boldsymbol{k}} u_n\rangle]$ has the meaning of the quantum metric in $(\boldsymbol{k}, E_\perp)$ space for a pair of bands n and m, in parallel to the familiar k-space quantum metric for a pair of bands [44–46] (see details in the Supplemental Material [39]). It is gauge invariant and related to the Fubini-Study metric [47] $\boldsymbol{g}^n = {\rm Re}\langle\partial_{E_\perp} u_n|(1 - |u_n\rangle\langle u_n|)|\partial_{\boldsymbol{k}} u_n\rangle$ in $(\boldsymbol{k}, E_\perp)$ space as $\boldsymbol{g}^n = \sum_{m\neq n}\boldsymbol{g}^{nm}$. Moreover, $\chi^{\rm int}$ can be decomposed into the Fubini-Study metric term plus an additional interband contribution (AIC),

$$\chi^{\rm int} = 2\hbar e^2 \sum_n \int \frac{d\boldsymbol{k}}{(2\pi)^2}\frac{\partial f_0}{\partial \varepsilon_n}\frac{(\boldsymbol{v}^n \times \boldsymbol{g}^n)_z}{\varepsilon_n - \varepsilon_{\bar{n}}} + \chi^{\rm int}_{\rm AIC}, \tag{8}$$

where $\boldsymbol{v}^n = \partial\varepsilon_n/\hbar\partial\boldsymbol{k}$, and $\bar{n}$ denotes the band whose energy is closest to n. In both tTMD and TBG, we find that the Fubini-Study metric term strongly dominates [shown below in Figs. 1(b) and 1(c) and Figs. 3(e) and 3(f)].

Phase tunable Hall rectification. This effect can be utilized for the rectification and frequency doubling of an in-plane ac input $\boldsymbol{E}_\parallel = \boldsymbol{E}^0_\parallel \cos\omega t$, provided that the out-of-plane field has the same frequency, namely $E_\perp = E^0_\perp \cos(\omega t + \varphi)$. The phase difference φ between the two fields plays an important role in determining the Hall current, which takes the form of

$$\boldsymbol{j} = \boldsymbol{j}^0 \sin\varphi + \boldsymbol{j}^{2\omega}\sin(2\omega t + \varphi). \tag{9}$$

Here, ω is required to be below the threshold for direct interband transition in order to validate the semiclassical treatment, and

$$\boldsymbol{j}^0 = \boldsymbol{j}^{2\omega} = \sigma_{\rm H}\hat{\boldsymbol{z}} \times \boldsymbol{E}^0_\parallel, \tag{10}$$

where $\sigma_{\rm H} = \frac{1}{2}\omega E^0_\perp \chi^{\rm int}$ quantifies the Hall response with respect to the in-plane input.

One notes that the rectified output is allowed only if the two crossed driving fields are not in phase or antiphase. Its on/off, chirality (right or left), and magnitude are all controlled by the phase difference of the two fields. Such a unique tunability provides not only a prominent experimental hallmark of this effect, but also a controllable route to Hall rectification. In addition, reversing the direction of the out-of-plane field switches that of the Hall current, which also serves as a control knob.

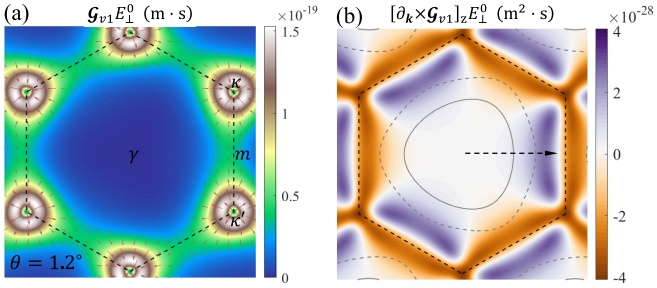

FIG. 2. (a) The interlayer BCP $\boldsymbol{\mathcal{G}}$, and (b) its vorticity $[\partial_{\boldsymbol{k}} \times \boldsymbol{\mathcal{G}}]_z$ on the first valence band from the $+K$ valley of 1.2° $tMoTe_2$. The background color and arrows in (a) denote the magnitude and vector flow, respectively. Gray curves in (b) show energy contours at 1/2 and 3/4 of the bandwidth. The black dashed arrow denotes the direction of increasing hole-doping level. The black dashed hexagons in (a) and (b) denote the boundary of the moiré Brillouin zone (mBZ).

Application to tTMDs. We now study the effect quantitatively in tTMDs, using $tMoTe_2$ as an example [31,32] (see details of the continuum model in Ref. [43]). For illustrative purposes, we take $\omega/2\pi = 0.1$ THz and $E^0_\perp d_0 = 10$ mV [21,26,27] in what follows.

Figures 1(b) and 1(c) present the electronic band structures at twist angles $\theta = 1.2°$ and $\theta = 2°$. In both cases, the energy spectra exhibit isolated narrow bands with strong layer hybridization. At $\theta = 1.2°$, the conductivity shows two peaks $\sim 0.1e^2/h$ at low energies associated with the first two valence bands. At higher hole-doping levels, a remarkable conductivity peak $\sim e^2/h$ appears near the gap separating the fourth and fifth bands. At $\theta = 2°$, the conductivity shows smaller values, but the overall trends are similar: A peak $\sim O(0.01)e^2/h$ appears at low energies, while larger responses $\sim O(0.1)e^2/h$ can be spotted as the Fermi level decreases.

One can understand the behaviors of $\sigma_{\rm H}$ from the interlayer BCP in Eq. (4). It favors band near-degeneracy regions in k space made up of strongly layer hybridized electronic states. As such, the conductivity is most pronounced when the Fermi level is located around such regions, which directly accounts for the peaks of response in Fig. 1(b) [and Fig. 1(c)]. When the Fermi level is located on the third valence band in Fig. 1(b), the effect is vanishingly small due to the large gaps to adjacent bands.

Let us take the case of the Fermi level being located within the first valence band of 1.2° $tMoTe_2$ in Fig. 1(b) as an example and explain the emergence of the first conductivity peak. The k-space distributions of $\boldsymbol{\mathcal{G}}$ and $[\partial_{\boldsymbol{k}} \times \boldsymbol{\mathcal{G}}]_z$ for this band are shown in Figs. 2(a) and 2(b), respectively. $\boldsymbol{\mathcal{G}}$ is suppressed around the corners of mBZ, because the states are strongly layer polarized there. Interlayer hybridization becomes stronger as $\boldsymbol{k}$ moves away from the mBZ corners. In this process, the competition between enlarged $p^{nm}(\boldsymbol{k})$ and k-space local gap renders narrow ringlike structures enclosing

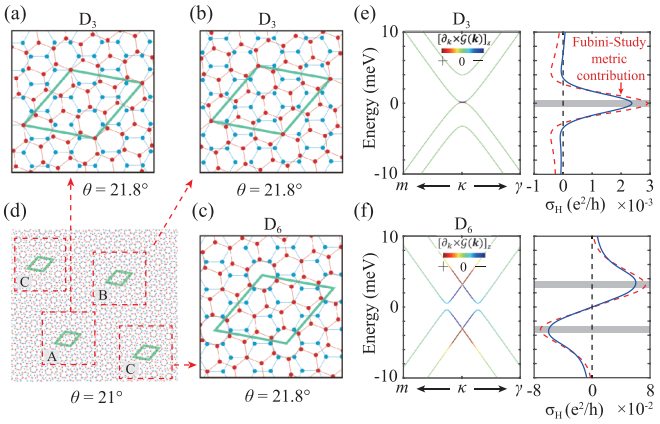

FIG. 3. (a)–(c) Three high-symmetry stacking registries for tBG with a commensurate twist angle $\theta = 21.8^\circ$. Lattice geometries with a rotation center on an overlapping atomic site (a), (b) and hexagonal center (c). (d) Schematic of the moiré pattern when the twist angle slightly deviates from 21.8°, here $\theta = 21^\circ$. Red squares marked by A–C are the local regions that resemble commensurate 21.8° patterns in (a)–(c), respectively. (e), (f) Low-energy band structures and intrinsic Hall conductivity of the two geometries [(a) and (b) are equivalent]. The red dashed curve denotes the contribution of the Fubini-Study metric term. The shaded areas highlight energy windows $\sim\hbar\omega$ around band degeneracies where interband transitions, not considered here, may quantitatively affect the conductivity measured.

the mBZ corners, in which $\boldsymbol{\mathcal{G}}$ is prominent and points radially inward/outward around κ/κ'. The distribution of $\boldsymbol{\mathcal{G}}$ dictates that of $[\partial_{\boldsymbol{k}} \times \boldsymbol{\mathcal{G}}]_z$. One observes that $[\partial_{\boldsymbol{k}} \times \boldsymbol{\mathcal{G}}]_z$ is negligible at lower energies, and it is dominated by positive values as the doping increases, thus the conductivity rises initially. As the doping level is higher, regions of $[\partial_{\boldsymbol{k}} \times \boldsymbol{\mathcal{G}}]_z < 0$ start to contribute, thus the conductivity decreases after reaching a maximum.

Application to tBG. The second example is tBG. We focus on commensurate twist angles in the large angle limit in the main text [48], which possess moiré-lattice-assisted strong interlayer tunneling via umklapp processes [49]. This case is appealing because the umklapp interlayer tunneling is a manifestation of the discrete translational symmetry of a moiré superlattice, which is irrelevant at small twist angles and not captured by the continuum model but plays important roles in physical contexts such as higher-order topological insulators [50] and moiré excitons [51–53]. The umklapp tunneling is strongest for the commensurate twist angles of $\theta = 21.8^\circ$ and $\theta = 38.2^\circ$, whose corresponding periodic moiré superlattices have the smallest lattice constant ($\sqrt{7}$ of the monolayer counterpart). Such a small moiré scale implies that the exact crystalline symmetry, which depends sensitively on the fine details of the rotation center, has a critical influence on the low-energy response properties.

To capture the umklapp tunneling, we employ the tight-binding model [48]. Figures 3(a)–3(c) show two distinct commensurate structures of tBG at $\theta = 21.8^\circ$ belonging to chiral point groups D_3 and D_6, respectively. The atomic configurations in Figs. 3(a) and 3(b) are equivalent, which are constructed by twisting AA-stacked bilayer graphene around an overlapping atom site, and that in Fig. 3(c) is obtained by rotating around a hexagonal center. The band structures of these two configurations are drastically different within a low-energy window of $\sim$10 meV around the κ point [48]. Remarkably, despite large θ, we still get $\sigma_{\rm H} \sim O(0.001)\, e^2/h$ (D_3) and $\sim O(0.1)\, e^2/h$ (D_6), which are comparable to those at small angles (cf. Fig. S1 in Supplemental Material [39]). Such sizable responses can be attributed to the strong interlayer coupling enabled by umklapp processes [43,51–53]. The profiles of $\sigma_{\rm H}$ can be understood from the distribution of $[\partial_{\boldsymbol{k}} \times \boldsymbol{\mathcal{G}}]_z$.

Figure 3(d) illustrates the atomic structure of tBG with a twist angle slightly deviating from $\theta = 21.8^\circ$, forming a supermoiré pattern [39]. In short range, the local stacking geometries resemble the commensurate configurations at $\theta = 21.8^\circ$, while the stacking registries at different locales differ by a translation. Similar to the moiré landscapes in the small-angle limit, high-symmetry locales also exist: Regions A and B enclose the D_3 structure, and region C contains the D_6 configuration. A position-dependent Hall response is therefore expected in such a supermoiré. As the intrinsic Hall signal from the D_6 configuration dominates [see Figs. 3(e) vs 3(f)], the net response mimics that in Fig. 3(f). As the twist angle deviates more from 21.8°, both the scales of supermoiré and of the D_3 and D_6 local regions become shorter.

Discussion. We have uncovered the intrinsic crossed nonlinear dynamical Hall effect characteristic of layer hybridized electrons in twisted bilayers, elucidated its quantum geometric origin, and showed its sizable values in tTMD and tBG. Our focus is on the intrinsic effect, which can be evaluated quantitatively for each material and provides a benchmark for experiments. There may also be extrinsic contributions, similar to the side jump and skew scattering in the anomalous Hall effect. They typically have a distinct scaling behavior with the relaxation time τ from the intrinsic effect, hence can be distinguished from the latter in experiments [3,5,12,54]. Moreover, they are suppressed in the clean limit $\omega\tau \gg 1$ [12]. In high-quality tBG, $\tau \sim$ ps at room temperature [55]. Much longer τ can be obtained at lower temperatures. In fact, a recent theory explaining well the resistivity of tBG predicted $\tau \sim 10^{-8}$ s at 10 K [56]. As such, high-quality tBG under low temperatures and subterahertz input ($\omega/2\pi = 0.1$ THz) is located in the clean limit, rendering an ideal platform for isolating the intrinsic effect.

This work paves a different route to driving the in-plane response by the out-of-plane dynamical control of layered vdW structures [57]. The study can be generalized to other observables such as spin current and spin polarization, and the in-plane driving can be statistical forces, such as the temperature gradient. Such orthogonal controls rely critically on the nonconservation of the layer pseudospin degree of freedom, and constitute an emerging research field at the crossing of vdW materials, layertronics, twistronics, and nonlinear electronics.

Acknowledgments. This work is supported by the National Key R&D Program of China (Grant No. 2020YFA0309600), the Research Grant Council of Hong Kong (AoE/P-701/20, HKU SRFS2122-7S05), the Croucher Foundation, and New Cornerstone Science Foundation. C.X. also acknowledges support by the UM Start-up Grant (SRG2023-00033-IAPME).

[1] I. Sodemann and L. Fu, Quantum nonlinear Hall effect induced by Berry curvature dipole in time-reversal invariant materials, Phys. Rev. Lett. **115**, 216806 (2015).

[2] Q. Ma, S. Y. Xu, H. Shen, D. MacNeill, V. Fatemi, T. R. Chang, A. M. Mier Valdivia, S. Wu, Z. Du, C. H. Hsu, S. Fang, Q. D. Gibson, K. Watanabe, T. Taniguchi, R. J. Cava, E. Kaxiras, H. Z. Lu, H. Lin, L. Fu, N. Gedik *et al.*, Observation of the nonlinear Hall effect under time-reversal-symmetric conditions, Nature (London) **565**, 337 (2019).

[3] K. Kang, T. Li, E. Sohn, J. Shan, and K. F. Mak, Nonlinear anomalous Hall effect in few-layer WTe_2, Nat. Mater. **18**, 324 (2019).

[4] Z. Z. Du, H. Z. Lu, and X. C. Xie, Nonlinear Hall effects, Nat. Rev. Phys. **3**, 744 (2021).

[5] S. Lai, H. Liu, Z. Zhang, J. Zhao, X. Feng, N. Wang, C. Tang, Y. Liu, K. S. Novoselov, S. A. Yang, and W.-b. Gao, Third-order nonlinear Hall effect induced by the Berry-connection polarizability tensor, Nat. Nanotechnol. **16**, 869 (2021).

[6] J. Zhou, W. Zhang, Y. C. Lin, J. Cao, Y. Zhou, W. Jiang, H. Du, B. Tang, J. Shi, B. Jiang, X. Cao, B. Lin, Q. Fu, C. Zhu, W. Guo, Y. Huang, Y. Yao, S. S. P. Parkin, J. Zhou, Y. Gao *et al.*, Heterodimensional superlattice with in-plane anomalous Hall effect, Nature (London) **609**, 46 (2022).

[7] Y. Zhang and L. Fu, Terahertz detection based on nonlinear Hall effect without magnetic field, Proc. Natl. Acad. Sci. USA **118**, e2100736118 (2021).

[8] D. F. Shao, S. H. Zhang, G. Gurung, W. Yang, and E. Y. Tsymbal, Nonlinear anomalous Hall effect for Néel vector detection, Phys. Rev. Lett. **124**, 067203 (2020).

[9] P. He, G. K. W. Koon, H. Isobe, J. Y. Tan, J. Hu, A. H. C. Neto, L. Fu, and H. Yang, Graphene moiré superlattices with giant quantum nonlinearity of chiral Bloch electrons, Nat. Nanotechnol. **17**, 378 (2022).

[10] J. Duan, Y. Jian, Y. Gao, H. Peng, J. Zhong, Q. Feng, J. Mao, and Y. Yao, Giant second-order nonlinear Hall effect in twisted bilayer graphene, Phys. Rev. Lett. **129**, 186801 (2022).

[11] N. Nagaosa, J. Sinova, S. Onoda, A. H. MacDonald, and N. P. Ong, Anomalous Hall effect, Rev. Mod. Phys. **82**, 1539 (2010).

[12] Z. Z. Du, C. M. Wang, S. Li, H. Z. Lu, and X. C. Xie, Disorder-induced nonlinear Hall effect with time-reversal symmetry, Nat. Commun. **10**, 3047 (2019).

[13] Y. Gao, S. A. Yang, and Q. Niu, Field induced positional shift of Bloch electrons and its dynamical implications, Phys. Rev. Lett. **112**, 166601 (2014).

[14] T. Holder, D. Kaplan, and B. Yan, Consequences of time-reversal-symmetry breaking in the light-matter interaction: Berry curvature, quantum metric, and diabatic motion, Phys. Rev. Res. **2**, 033100 (2020).

[15] C. Wang, Y. Gao, and D. Xiao, Intrinsic nonlinear Hall effect in antiferromagnetic tetragonal CuMnAs, Phys. Rev. Lett. **127**, 277201 (2021).

[16] H. Liu, J. Zhao, Y. X. Huang, W. Wu, X. L. Sheng, C. Xiao, and S. A. Yang, Intrinsic second-order anomalous Hall effect and its application in compensated antiferromagnets, Phys. Rev. Lett. **127**, 277202 (2021).

[17] F. Mazzola, B. Ghosh, J. Fujii, G. Acharya, D. Mondal, G. Rossi, A. Bansil, D. Farias, J. Hu, A. Agarwal, A. Politano, and I. Vobornik, Discovery of a magnetic Dirac system with a large intrinsic nonlinear Hall effect, Nano Lett. **23**, 902 (2023).

[18] L. Xiang, C. Zhang, L. Wang, and J. Wang, Third-order intrinsic anomalous Hall effect with generalized semiclassical theory, Phys. Rev. B **107**, 075411 (2023).

[19] A. Gao, Y. F. Liu, J. X. Qiu, B. Ghosh, T. V. Trevisan, Y. Onishi, C. Hu, T. Qian, H. J. Tien, S. W. Chen *et al.*, Quantum metric nonlinear Hall effect in a topological antiferromagnetic heterostructure, Science **381**, 181 (2023).

[20] N. Wang, D. Kaplan, Z. Zhang, T. Holder, N. Cao, A. Wang, X. Zhou, F. Zhou, Z. Jiang, C. Zhang *et al.*, Quantum metric-induced nonlinear transport in a topological antiferromagnet, Nature (London) **621**, 487 (2023).

[21] E. Y. Andrei and A. H. MacDonald, Graphene bilayers with a twist, Nat. Mater. **19**, 1265 (2020).

[22] L. Balents, C. R. Dean, D. K. Efetov, and A. F. Young, Superconductivity and strong correlations in moiré flat bands, Nat. Phys. **16**, 725 (2020).

[23] D. M. Kennes, M. Claassen, L. Xian, A. Georges, A. J. Millis, J. Hone, C. R. Dean, D. N. Basov, A. N. Pasupathy, and A. Rubio, Moiré heterostructures as a condensed-matter quantum simulator, Nat. Phys. **17**, 155 (2021).

[24] E. Y. Andrei, D. K. Efetov, P. Jarillo-Herrero, A. H. MacDonald, K. F. Mak, T. Senthil, E. Tutuc, A. Yazdani, and A. F. Young, The marvels of moiré materials, Nat. Rev. Mater. **6**, 201 (2021).

[25] C. N. Lau, M. W. Bockrath, K. F. Mak, and F. Zhang, Reproducibility in the fabrication and physics of moiré materials, Nature (London) **602**, 41 (2022).

[26] N. P. Wilson, W. Yao, J. Shan, and X. Xu, Excitons and emergent quantum phenomena in stacked 2D semiconductors, Nature (London) **599**, 383 (2021).

[27] E. C. Regan, D. Wang, E. Y. Paik, Y. Zeng, L. Zhang, J. Zhu, A. H. MacDonald, H. Deng, and F. Wang, Emerging exciton physics in transition metal dichalcogenide heterobilayers, Nat. Rev. Mater. **7**, 778 (2022).

[28] P. San-Jose, J. González, and F. Guinea, Non-Abelian gauge potentials in graphene bilayers, Phys. Rev. Lett. **108**, 216802 (2012).

[29] D. Pesin and A. H. MacDonald, Spintronics and pseudospintronics in graphene and topological insulators, Nat. Mater. **11**, 409 (2012).

[30] X. Xu, W. Yao, D. Xiao, and T. F. Heinz, Spin and pseudospins in layered transition metal dichalcogenides, Nat. Phys. **10**, 343 (2014).

[31] F. Wu, T. Lovorn, E. Tutuc, I. Martin, and A. H. MacDonald, Topological insulators in twisted transition metal dichalcogenide homobilayers, Phys. Rev. Lett. **122**, 086402 (2019).

[32] H. Yu, M. Chen, and W. Yao, Giant magnetic field from moiré induced Berry phase in homobilayer semiconductors, Natl. Sci. Rev. **7**, 12 (2020).

[33] D. Zhai and W. Yao, Layer pseudospin dynamics and genuine non-Abelian Berry phase in inhomogeneously strained moiré pattern, Phys. Rev. Lett. **125**, 266404 (2020).

[34] D. Xiao, M. C. Chang, and Q. Niu, Berry phase effects on electronic properties, Rev. Mod. Phys. **82**, 1959 (2010).

[35] C. Xiao, H. Liu, J. Zhao, S. A. Yang, and Q. Niu, Thermoelectric generation of orbital magnetization in metals, Phys. Rev. B **103**, 045401 (2021).

[36] C. Xiao, H. Liu, W. Wu, H. Wang, Q. Niu, and S. A. Yang, Intrinsic nonlinear electric spin generation in centrosymmetric magnets, Phys. Rev. Lett. **129**, 086602 (2022).

[37] D. J. Thouless, Quantization of particle transport, Phys. Rev. B **27**, 6083 (1983).
[38] D. Culcer and Q. Niu, Geometrical phase effects on the Wigner distribution of Bloch electrons, Phys. Rev. B **74**, 035209 (2006).
[39] See Supplemental Material at http://link.aps.org/supplemental/10.1103/PhysRevResearch.6.L012059 for the detailed derivations of Eqs. (3)–(5) and of the quantum metric related formulas, the effect in tBG with small twist angles, and the elaborated discussion on tBG with a twist angle around 21.8°, which includes Refs. [40,41].
[40] M. Koshino, N. F. Q. Yuan, T. Koretsune, M. Ochi, K. Kuroki, and L. Fu, Maximally localized Wannier orbitals and the extended Hubbard model for twisted bilayer graphene, Phys. Rev. X **8**, 031087 (2018).
[41] Z. Song, Z. Wang, W. Shi, G. Li, C. Fang, and B. A. Bernevig, All magic angles in twisted bilayer graphene are topological, Phys. Rev. Lett. **123**, 036401 (2019).
[42] Y. Gao, Y. Zhang, and D. Xiao, Tunable layer circular photogalvanic effect in twisted bilayers, Phys. Rev. Lett. **124**, 077401 (2020).
[43] D. Zhai, C. Chen, C. Xiao, and W. Yao, Time-reversal even charge Hall effect from twisted interface coupling, Nat. Commun. **14**, 1961 (2023).
[44] H. Watanabe and Y. Yanase, Chiral photocurrent in parity-violating magnet and enhanced response in topological antiferromagnet, Phys. Rev. X **11**, 011001 (2021).
[45] J. Ahn, G. Y. Guo, N. Nagaosa, and A. Vishwanath, Riemannian geometry of resonant optical responses, Nat. Phys. **18**, 290 (2022).
[46] P. Bhalla, K. Das, D. Culcer, and A. Agarwal, Resonant second-harmonic generation as a probe of quantum geometry, Phys. Rev. Lett. **129**, 227401 (2022).
[47] J. P. Provost and G. Vallee, Riemannian structure on manifolds of quantum states, Commun. Math. Phys. **76**, 289 (1980).
[48] P. Moon and M. Koshino, Optical absorption in twisted bilayer graphene, Phys. Rev. B **87**, 205404 (2013).
[49] E. J. Mele, Commensuration and interlayer coherence in twisted bilayer graphene, Phys. Rev. B **81**, 161405(R) (2010).
[50] M. J. Park, Y. Kim, G. Y. Cho, and S. B. Lee, Higher-order topological insulator in twisted bilayer graphene, Phys. Rev. Lett. **123**, 216803 (2019).
[51] H. Yu, Y. Wang, Q. Tong, X. Xu, and W. Yao, Anomalous light cones and valley optical selection rules of interlayer excitons in twisted heterobilayers, Phys. Rev. Lett. **115**, 187002 (2015).
[52] K. L. Seyler, P. Rivera, H. Yu, N. P. Wilson, E. L. Ray, D. G. Mandrus, J. Yan, W. Yao, and X. Xu, Signatures of moiré-trapped valley excitons in $MoSe_2/WSe_2$ heterobilayers, Nature (London) **567**, 66 (2019).
[53] L. Zhang, Z. Zhang, F. Wu, D. Wang, R. Gogna, S. Hou, K. Watanabe, T. Taniguchi, K. Kulkarni, T. Kuo, S. R. Forrest, and H. Deng, Twist-angle dependence of moiré excitons in $WS_2/MoSe_2$ heterobilayers, Nat. Commun. **11**, 5888 (2020).
[54] C. Xiao, H. Zhou, and Q. Niu, Scaling parameters in anomalous and nonlinear Hall effects depend on temperature, Phys. Rev. B **100**, 161403(R) (2019).
[55] L. Sun, Z. Wang, Y. Wang, L. Zhao, Y. Li, B. Chen, S. Huang, S. Zhang, W. Wang, D. Pei, H. Fang, S. Zhong, H. Liu, J. Zhang, L. Tong, Y. Chen, Z. Li, M. H. Rümmeli, K. S. Novoselov, H. Peng *et al.*, Hetero-site nucleation for growing twisted bilayer graphene with a wide range of twist angles, Nat. Commun. **12**, 2391 (2021).
[56] G. Sharma, I. Yudhistira, N. Chakraborty, D. Y. Ho, M. Al Ezzi, M. S. Fuhrer, G. Vignale, and S. Adam, Carrier transport theory for twisted bilayer graphene in the metallic regime, Nat. Commun. **12**, 5737 (2021).
[57] D. Zhai and W. Yao, Ultrafast control of moiré pseudo-electromagnetic field in homobilayer semiconductors, Nat. Sci. **2**, e20210101 (2022).